

Measuring, imaging and suppressing scattered surface waves

Xander H. Campman¹, Kasper van Wijk², John A. Scales² and Gérard C. Herman^{3,1}

¹ Dept of Applied Mathematical Analysis, Delft University of Technology, ² Physical Acoustic Laboratory at Colorado School of Mines, ³ Shell International E & P.

Summary

Near-surface scattering can contaminate the arrival of energy from target reflectors. We describe a 3D imaging method, as a multi-channel alternative for short-wavelength static corrections, that is tested on laboratory data, excited and monitored with a computer controlled, non-contacting system. Application of the algorithm improves the continuity of arrivals that have been disturbed by a cavity in the surface of the models.

Introduction

When a wave front travels through a complex overburden, it is disturbed by scattering from heterogeneities. For a detailed structural image of the deeper subsurface it is important to minimize these disturbances in arrival time and amplitude of upcoming reflections. Currently, residual static correction methods correct for rapid variations in arrival times of a reflector, but these techniques are based on a model that assigns the same uniform time shift to each trace from a distinct surface location (Wiggins et al., 1976, e.g.), assuming vertical ray paths through the overburden. Such corrections are usually referred to as time- and surface-consistent corrections (Taner et al., 1974). Although statics techniques are based on this simple (transmission) model of the subsurface, they can be effective in many cases, but in a strongly heterogeneous shallow subsurface, this statics model breaks down (Combee, 1994, e.g.). Neglecting (multiply) scattered waves, like in the static assumption, can degrade the high-frequency content of the data, due to destructive interference of rapidly varying traces during stacking. We estimate a surface impedance distribution of the region directly under the receivers from one particular event and subsequently predict and subtract the scattered energy for the entire record, improving resolution of the target reflectors. This method is based on an integral-equation formulation of the scattering process near the surface. We present examples based on laboratory models, where we excite and measure wave fields that are scattered at the near surface. With our non-contacting data acquisition, receiver intervals are less than the dominant wavelength, allowing us to filter in the wavenumber domain, like the dense receiver arrays that are currently being tested in exploration geophysics (Baeten et al., 2000).

Scattered noise model

The objective is to obtain an estimate of the complete wave field without scattered energy from near-surface

heterogeneities. On account of linearity of the elastic wave field, the vertical velocity component $v(\underline{x}, t)$, measured at position $\underline{x} = (x, y, z)$ and due to a fixed vertical point source of force type can be written as

$$v(\underline{x}, t) = v^0(\underline{x}, t) + v^1(\underline{x}, t). \quad (1)$$

Here, v is the measured field, v^0 is the field that would have been measured if the overburden were homogeneous and v^1 is the part of the wave field that accounts for scattering from heterogeneities close to the acquisition surface. Thus, we want an estimate of v^0 . Our approach is to find the scattered noise, v^1 , and then subtract it from the data as in Equation (1). From the elastic wave-equation for particle displacement, we can derive an approximate integral representation for the scattered noise in terms of the vertical component of particle velocity, measured at the surface z_0 :

$$v^1(\underline{x}_l, z_0, \omega) = \int_{\underline{x}'_l \in \Sigma} u^G(\underline{x}_l - \underline{x}'_l, \Delta z, \omega) \sigma(\underline{x}'_l, z_1, \omega) v(\underline{x}'_l, z_1, \omega) d\underline{x}'_l, \quad (2)$$

where u^G is the vertical component of the Green's displacement tensor, due to a vertical point force. Horizontal position is denoted by $\underline{x}_l = (x, y)$, z_1 is the scattering depth and $\Delta z = z_0 - z_1$. The impedance distribution is denoted by σ ; ω is angular frequency. The surface Σ is the area occupied by the receivers (i.e. the acquisition surface). If the scattering takes place close to the surface ($z_1 \approx z_0$), we can approximate the field at z_1 by the field recorded field at depth z_0 . We can calculate the scattered field v^1 once we know σ . Note that the integral is over a surface and we thus express scattering by a scattering volume in terms of a surface impedance distribution. The validity of this assumption for scattering of surface waves close to the surface is investigated in (Blonk and Herman, 1994). To account for variations in the actual depth of the scatterers we allow the impedance distribution to depend on frequency.

Inverse scattering

Suppose the data contain many reflections from deeper layers. All these events excite surface waves at the same heterogeneities close to the acquisition surface. This implies that we can use the scattered energy from a single event to estimate the impedance distribution and use it to predict the scattered energy on every reflection using Equation (2). In fact, this is comparable to residual statics methods, where one selects a strong reflection event from the data, to derive the time-shifts for each trace

Imaging scattered surface waves

separately. Instead of this single-channel operation, we now select one event to derive an impedance distribution to estimate the scattered energy (i.e. a multi-channel operation).

First, we select an event:

$$v(\underline{x}, t) = d(\underline{x}, t) + r(\underline{x}, t), \quad (3)$$

where v are the data, d is the selected event and r denotes the rest of the data. Selecting d can be done by time windowing. The window should be long enough to include scattering tails but it should not include other events. Next, we decompose the strong event $d(\underline{x}, t)$, in a similar way as in Equation (1):

$$d(\underline{x}, t) = d^0(\underline{x}, t) + d^1(\underline{x}, t). \quad (4)$$

Here, d^0 is the field in the near surface that would exist without scattering and d^1 is the scattered field, excited by the incident field being scattered from heterogeneities in the near surface. The scattered energy can be obtained via spatial filtering. This is discussed in more detail in the following examples. The impedance model is obtained from back-propagating the near-surface scattered energy with the Green's function. The impedance distribution is determined by minimizing an L^2 -norm, using conjugate gradient. To set up the minimization scheme, we write Equation (2) for a single event, in the form

$$d^1 = \mathcal{K}\sigma, \quad (5)$$

where σ is the surface impedance distribution and the operator \mathcal{K} is defined as

$$\{\mathcal{K}\sigma\}(\underline{x}_i, z_0, \omega) = \int_{\underline{x}'_i \in \Sigma} u^G(\underline{x}_i - \underline{x}'_i, \Delta z, \omega) \sigma(\underline{x}'_i, z_1, \omega) d(\underline{x}'_i, z_1, \omega) d\underline{x}'_i. \quad (6)$$

We then minimize the squared difference between the observed scattered field and the reconstructed scattered field, regularized by the norm of the distribution of scatterers:

$$F = \frac{\|d^1 - \mathcal{K}\sigma\|^2}{\|d^1\|^2} + \lambda \|\sigma\|^2, \quad (7)$$

where the size of λ determines the penalty on the norm of the distribution of scatterers. By assumption, the scatterers are close to the surface so that in Equation (6), we can substitute the field at depth z_1 with the field at z_0 , leaving σ the only unknown. In contrast to Born-type imaging methods, this method accounts for multiply scattered waves.

Description of experiment I

In the Physical Acoustics Laboratory at CSM we measure the wave field on the surface of an aluminum block, excited by a pulsed infrared laser. We focused the laser beam on a line to create a line surface wave source. This

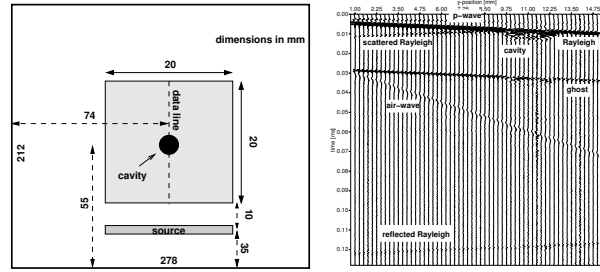


Fig. 1: (left) Top view of the aluminum block with cavity. The light shaded area is the area covered by the receivers. The source width (dark shade) is 0.5 mm. (right) In-line panel of the data. Events have been identified.

wave front is scattered by a cylindrical cavity with a diameter of 2 mm and a depth of 3 mm, which is also roughly the size of the dominant wavelength. The wave field is detected using a scanning laser interferometer that measures the vertical component of the particle velocity on the surface of the model via the Doppler shift (Scales and van Wijk, 1999). Traces are recorded at 0.25 mm intervals, which implies about 10 samples per wavelength. The left panel of Figure 1 is the top view of the experimental configuration, while the right panel is an in-line panel of the 3D data set, with several surface-wave events and a body wave (P-wave) identified. The quality of these data is such, that no pre-processing is required.

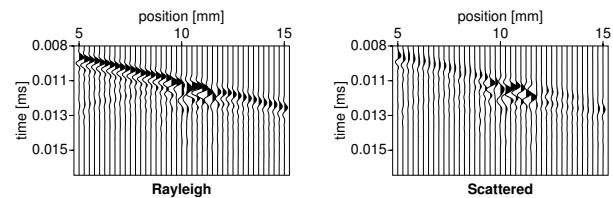


Fig. 2: (left) Part of the direct Rayleigh wave (event d in the text). This event is used to derive the scattered energy d^1 . (right) Separated scattered energy, d^1 , using a wavenumber-frequency filter.

Results of Experiment I

We use data from Experiment 1 to validate the algorithm. First, we select an event by time windowing; in this case the direct Rayleigh wave with the energy scattered by the cavity, plotted in the left panel of Figure 2. We separate the incoming (d^0) from the energy scattered by the cavity (d^1). To do so, we exploit the near-planar character of the incoming wave. Since a two-dimensional spatial Fourier transformation maps a plane wave to a point in the wavenumber-frequency domain, we can use this to separate the incoming plane wave from its local perturbations. These perturbations are attributed to the presence of the cavity. The separated scattered field d^1 is shown in the right panel of Figure 2.

Imaging scattered surface waves

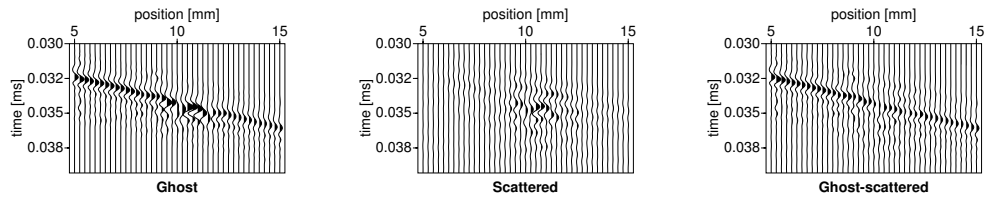


Fig. 3: (left) The ghost Rayleigh wave. (middle) The predicted scattered field, excited by the ghost. (right) The ghost Rayleigh wave, after removing near-surface scattering.

Next, we estimate the impedance distribution using Equation (7) and an independent estimate of the background velocity of the surface waves in aluminum. From the data, we estimate that $c_R \approx 3000$ m/s. A top-view of the estimated impedance distribution at $t = 0$, for the entire 3D data volume, is shown in the left panel of Figure 6. The circular shape of the impedance distribution, slightly to the left and down from center, represents the actual shape and location of the cavity. Anomalies in the right corners of the figure are due to local data quality issues. Having obtained an estimate of the spatial impedance distribution from the direct Rayleigh wave, we calculate the scattered wave field v^1 for a *different* event. This event has not been used for determining the impedance distribution, and therefore prediction of the scattered field is a good test of the method. We select the Rayleigh wave that is reflected by the end of the aluminum block behind the source. We call this event the “ghost,” shown in the left panel of Figure 3. The predicted scattered field is shown in the middle panel of Figure 3. Finally, we obtain the wave field minus the scattered energy from Equation (1), shown in the right panel of Figure 3. We observe that the scattering has been effectively removed and continuity of the reflector has increased.

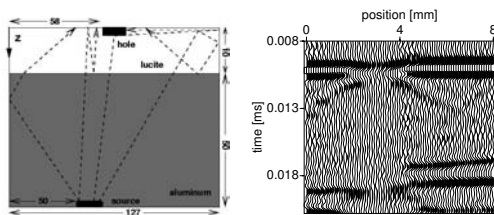


Fig. 4: (left) Side-view of the two-layered model with cavity. (right) Seismogram through the cavity from left to right.

Description of experiment II

In order to simulate an upcoming reflection, Experiment 2 involves a transmission model. Body waves are excited at the bottom of a two-layered model, where an aluminum layer is topped by a Lucite layer, in which we drilled a 2-mm wide and 3-mm deep cavity. When the body waves reach the surface, energy is scattered at the cavity. We record the wave field in a 4 cm^2 region, at 0.1 mm intervals. Compared to Experiment 1, these data

are further complicated by the fact that they contain multiples from the layer boundary and reflections from the sides of the aluminum block as depicted in the side-view in the left panel of Figure 4. Data through the cavity show the multiples between the layers, reflections from the sides, all scattered by the cavity (right panel of Figure 4). Some pre-processing was required in order to improve the signal-to-noise ratio.

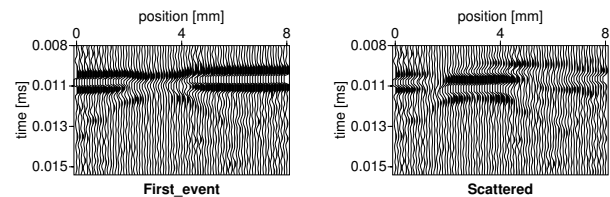


Fig. 5: (left) The first upcoming event from the data. (event d in the text). This event is used to derive the scattered energy d^1 . (right) Separated scattered energy, d^1 , using a narrow wavenumber-frequency domain filter.

Results of Experiment II

The data in Experiment 2 present a more challenging test for the method because of the multiples and the interfering reflections from the sides of the aluminum. Apart from the pre-processing of these data, the algorithm is applied in the same way as in Experiment 1. Again, we start by selecting a clear event. In this case we select the first upcoming reflection, shown in the left panel of Figure 5.

We separate the incoming (d^0) from the energy scattered by the cavity (d^1), using a narrow wavenumber-frequency domain filter. The separated scattered field is shown in the right panel. Using the surface-wave velocity in Lucite ($c_R \approx 1000$ m/s), we estimate the impedance distribution, shown in the right panel. Figure 6 is a top-view of the image at the surface for the entire 3D data volume. The dimensions and location of the image are in agreement with the actual cavity in the Lucite. Finally, we predict the near-surface scattered field in the rest of the data. In the left panel of Figure 7 we show part of a line crossing through the cavity, minus the first event used to construct the image. Thus, the data shown in the left panel of Figure 7 were not used to derive the impedance distribution. Because the surface-wave velocity may not be accurately known, the desired result may contain residual tails from surface waves, but these can be removed by dip filtering.

Imaging scattered surface waves

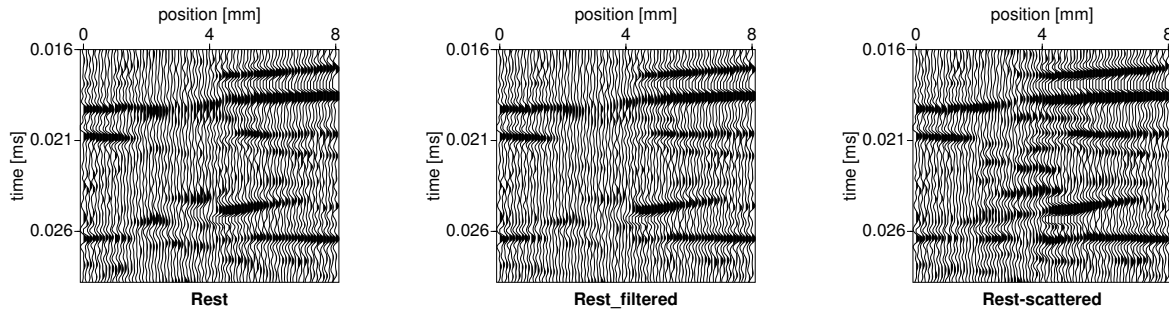


Fig. 7: (left) Part of the rest of the record. (middle) Same as in (left) but after dip-filtering to attenuate surface waves. (right) Rest of the record after subtracting near-surface scattered energy and after dip-filtering.

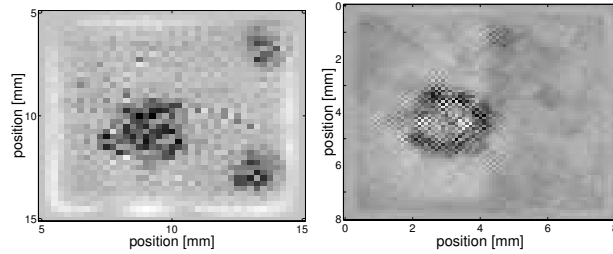


Fig. 6: (left) Top view of the image at $t = 0$ for the surface wave experiment, showing the right position of the cavity and two irregularities in the aluminum, at the right corners. (right) Same for transmission experiment.

In order to make a comparison between the data before and after applying the algorithm, we have used a dip filter on the input data v as well as in the output data v^0 . The filtered input data are shown in the middle panel of Figure 7. Obviously, the dip filter only removed the flanks of the surface waves, but not the apices, which have higher apparent velocities and were therefore unaffected by the filter. Especially this part of the surface waves is important to remove, because it is the interference between surface wave scattering and the incident field that diminishes the quality of the target reflector. The output v^0 after applying *the same* dip-filter is shown in the right panel of Figure 7. We conclude that the algorithm has improved the continuity of the reflectors.

Conclusions

We discuss a prediction-and-removal algorithm to attenuate strong near-surface scattering from seismic data. Using data from a laboratory-scale surface wave scattering experiment, we are able to estimate a surface impedance distribution from the direct Rayleigh wave and use this impedance to predict the scattered field excited by the ghost Rayleigh wave. By subtracting the predicted scattered field we restore the continuity of the ghost, while it was *not* used to estimate the impedance distribution. A similar test on a more challenging multiple scattering experiment also gives promising results.

Acknowledgments

Part of the work presented in this paper was carried out while XC was a visitor in the Physical Acoustics Laboratory (PAL) at Colorado School of Mines. He would like to thank everyone at PAL and the Center for Wave Phenomena for their hospitality and many fruitful discussions. The work of XC was supported by the Dutch Technology Foundation (STW). Part of the work at PAL was supported by the National Science Foundation (EAR-0111804) and the US Army Research Office (DAAG55-98-1-0070).

References

- Baeten, G., Belougne, V., Combee, L., Kragh, E., Laake, A., Martin, J., Orban, J., Ozbek, A., and Vermeer, P. L., 2000, Acquisition and processing of point receiver measurements in land seismic: 62nd Mtg., Expanded abstracts.
- Blonk, B., and Herman, G. C., 1994, Inverse scattering of surface waves : A new look at surface consistency: *Geophysics*, **59**, 963–972.
- Combee, L., 1994, Wavefield scattering by a 2-D near-surface elliptic anomaly: 64th Ann. Intern. Mtg., Expanded Abstracts, 1306–1309.
- Scales, J. A., and van Wijk, K., 1999, Multiple scattering attenuation and anisotropy of ultrasonic surface waves: *Applied Physics Letters*, **74**, 3899–3901.
- Taner, M. T., Koehler, F., and Alhilali, K. A., 1974, Estimation and correction of near-surface time anomalies: *Geophysics*, **39**, 441–463.
- Wiggins, R. A., Larner, K. L., and Wisecup, R. D., 1976, Residual statics analysis as a general linear inverse problem: *Geophysics*, **41**, 922–938.